Cellulose (2025) 32:2779–2791
https://doi.org/10.1007/s10570-024-06355-0

COMMUNICATION

Positrons as microprobes to study water-dependent free volume of wood cell walls: a preliminary study

Filip Majstorović · Eric Hirschmann · Maik Butterling · Ahmed G. Attallah · Andreas Wagner · Joseph E. Jakes

Received: 25 July 2024 / Accepted: 23 December 2024 / Published online: 29 January 2025

Abstract Positron annihilation lifetime spectroscopy (PALS) was employed to study the water-dependent free volume characteristics of wood cell walls in earlywood and latewood of loblolly pine (*Pinus taeda*). Measurements were conducted across relative humidity levels (1–80% RH) at room temperature, demonstrating good reproducibility and consistency with polymer science principles. The Tao-Eldrup model was applied to the measured ortho-positronium lifetimes to estimate the mean sizes of free volume elements in wood cell walls. At low relative humidity (below ~ 11%), water absorption resulted in antiplasticization, evidenced by a decrease in mean free volume element sizes. As relative humidity increased, water started acting as a plasticizer, causing the free volume elements to expand. While dry cell walls showed no significant differences in free volume element sizes between earlywood and latewood, earlywood exhibited larger mean free volume element sizes at all higher relative humidity levels. At higher relative humidity levels (above ~ 70% RH), the ortho-positronium lifetimes of cell wall free volume elements overlapped with those of liquid water, indicating PALS cannot provide reliable free volume information at higher cell wall moisture contents. Interpreting the intensity of ortho-positronium annihilation was complicated by the possibility of water inhibiting ortho-positronium formation in wood cell walls.

Keywords Positron annihilation · Free volume · Wood · Cell wall · Water · Biopolymer

Supplementary Information The online version contains supplementary material available at https://doi.org/10.1007/s10570-024-06355-0.

F. Majstorović (✉)
Fraunhofer Institute for Wood Research, Wilhelm-Klauditz-Institut WKI, 38108 Brunswick, Germany
e-mail: filip.majstorovic@wki.fraunhofer.de

F. Majstorović
Faculty of Mathematics, Natural Sciences and Information Technologies, University of Primorska, 6000 Koper, Slovenia

E. Hirschmann · M. Butterling · A. G. Attallah · A. Wagner
Institute of Radiation Physics, Helmholtz-Zentrum Dresden-Rossendorf, 01328 Dresden, Germany

A. G. Attallah
Physics Department, Faculty of Science, Minia University, Minia 61519, Egypt

J. E. Jakes
Forest Biopolymers Science and Engineering, USDA Forest Service, Forest Products Laboratory, One Gifford Pinchot Drive, Madison, WI 53726, USA

Introduction

Water within the wood cell wall structure (Fig. 1) has a major influence on the physical properties of wood and the performance of wood-based materials. Water molecules can plasticize the cell wall

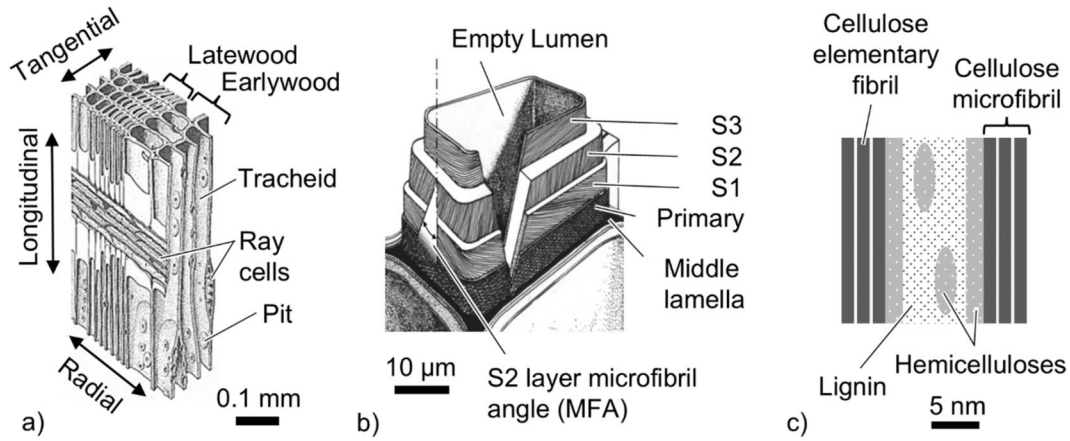

Fig. 1 Breakdown of softwood structure representative of the loblolly pine samples used in this study. **a** Anisotropic cellular structure with tangential and radial directions defining the transverse plane and the longitudinal direction parallel to the wood grain. Earlywood has thinner cell walls and larger lumina, whereas latewood is a denser material with thicker cell walls and smaller lumina (Wiedenhoeft and Miller 2005). **b** Tracheid walls consist of three secondary cell wall layers (S1, S2, and S3), and the thin primary cell wall layer. Secondary cell walls are fiber-reinforced composite structures with cellulose microfibrils wound helically around the tracheid. Tracheids are held together by the lignin-rich middle lamella (Rowell et al. 2012). **c** Within secondary cell walls, cellulose microfibrils are composed of semi-crystalline elementary fibrils and embedded in an organized matrix of hemicelluloses and lignin (Terashima et al. 2009)

polymers, i.e., amorphous cellulose, hemicelluloses, and lignin, and break inter-polymer chain hydrogen bonds, resulting in swelling of the polymer structure (Arzola-Villegas et al. 2019). In hydrophilic polymers, such as those making up the wood cell walls, the water-induced swelling is generally associated with an increase in polymer free volume, i.e., the volume of the polymer matrix not occupied by matter (Hodge et al. 1996). In other words, the small plasticizing water molecules create more empty space within the amorphous cell wall polymer regions than they occupy. These changes in cell wall free volume caused by water sorption affect the mobility of polymer chain segments, as shown by the various wood polymer thermal transitions that are affected by moisture content (Lenth and Kamke 2001). Many important wood properties are controlled by these molecular motions and thermal transitions. Under high enough moisture and temperature, lignin goes through a glass transition, and bulk wood mechanically softens (Jakes et al. 2019). Other wood cell wall properties dependent on free volume include water sorption (Thybring et al. 2019) and moisture-dependent molecular diffusion (Jakes et al. 2019). Water sorption causes swelling and shrinking in wood, leading to cracking, warping, and wood-adhesive bondline failures in wood composites (Glass and Zelinka 2010; Hunt et al. 2018). Molecular diffusion through wood cell walls is essential for industrial processes involving chemical diffusion into wood cell walls (e.g., biorefinery pretreatments and wood chemical modifications) and has also been linked to degradation caused by decay fungi (Ringman et al., 2019)

Despite the aforementioned importance of free volume in wood and wood-based materials, there is a lack of experimental studies describing the water-dependent free volume of intact wood or other lignocellulosic cell walls. This is primarily due to the limited availability of the equipment capable of probing both length (10^{-10} m) and time scales (as low as 10^{-9} s above glass transition) relevant to polymer molecular structure and its dynamics. Furthermore, precise control of relative humidity (RH) around the wood, essential for reliable studies of water-dependent wood properties, is challenging and sometimes impossible with certain methods. These experimental limitations have led to the application of atomistic modeling approaches to study the moisture-dependent free volume of cell wall polymers and associated mechanisms (Kulasinski et al. 2015; Kulasinski and Guyer 2016; Youssefian et al. 2017; Chen et al. 2018; Zhang

et al. 2021). While these studies provide valuable new insights into the cell wall ultrastructure, they often rely on simplified cell wall models and assumptions to reduce computational complexity and would benefit from further experimental validation.

The purpose of this brief report is to assess the suitability of positron annihilation lifetime spectroscopy (PALS) for water-dependent free volume measurements of wood. PALS is a radiation-based spectroscopy technique that uses positrons (antiparticles of electrons (e^+)) as subatomic probes to investigate defects within the material down to the atomic level (Schrader and Jean 1988; Hautojärvi 2012). During the experiment, positrons are generated by the radioactive decay of neutron-deficient nuclides (most commonly ^{22}Na) and are subsequently injected into the studied material. Once injected, the positron reaches thermal equilibrium almost instantly and continues to diffuse within the material with a diffusion length of approximately 200 nm in the case of polymers (Suzuki et al. 2010). During its residence within a low free electron density material having free volume elements of at least ~ 0.2 nm, e.g., polymers (Zgardzińska and Goworek 2013), the thermalized positron exists either as a free positron (e^+) or forms a positron–electron hydrogen-like bound state, i.e., a positronium (Ps) (Ruark 1945). Depending on the relative spin orientations of the positron and electron, the Ps can form either in para (p-Ps) or ortho (o-Ps) states, which differ in their lifetimes in vacuum (125 ps and 142 ns, respectively).

While the lifetime of p-Ps is not significantly affected by the material´s structure, o-Ps tends to get trapped in regions of reduced electron densities, such as voids, which substantially shortens its lifetime. In polymers, these voids represent individual free volume elements arising from irregular chain packing and molecular motions of polymer chain segments. Once trapped within a free volume element, the o-Ps will eventually annihilate due to its wavefunction overlapping with the surrounding electrons of the polymer. The wavefunction overlap is high in smaller free volume elements, leading to a shorter o-Ps lifetime. Conversely, larger free volume elements will result in longer o-Ps lifetimes. In other words, the o-Ps lifetime is directly related to the size of the free volume element in which o-Ps annihilation occurs.

Since positron generation and subsequent o-Ps annihilation in free volume elements are associated with defined gamma radiation in source-based PALS measurements, o-Ps lifetimes can be measured directly. This is achieved using photomultiplier tubes coupled with scintillation crystals (e.g., $CeBr_3$) connected to a digital signal acquisition setup capable of resolving these events occurring picoseconds apart. PALS experiments typically involve measuring tens of millions of positron annihilation events, generating a positron annihilation lifetime spectrum that contains information about the lifetimes (decay rate) of both free positrons (e^+) and positronium (p-Ps and o-Ps). Since only the o-Ps provides information about the polymer free volume, its lifetimes and corresponding intensities must be extracted from the PALS spectrum. Subsequently, the measured o-Ps lifetimes (in ns) can be converted into free volume element sizes and their distribution (in nm) using the quantum mechanical Tao-Eldrup model (Tao 1972; Eldrup et al. 1981). Furthermore, the intensity of the o-Ps annihilation is associated with the relative number of the probed free volume elements compared to an initial state (in the absence of any chemical reactions, e.g., spin conversion or spin flip).

Despite demonstrating the ability to provide useful data related to the free volume characteristics of polymers (Jean et al. 2013) and their composites (Sharma and Pujari 2017), most PALS studies so far have been focused on synthetic polymers. The small fraction of PALS literature covering polymers derived from natural resources is primarily based on polysaccharide matrices (De Yao et al. 1998; Kilburn et al. 2005; Sharma et al. 2011; Fukuzumi et al. 2011; Edlund et al. 2012; Roussenova and Alam 2013; Torstensen et al. 2018) and paper (Resch et al. 2022), which are much simpler than the wood cell wall in terms of their physical and chemical structure. We believe PALS can be a viable alternative to traditional probe-based techniques such as gas sorption solute exclusion methods. The important advantage of the o-Ps probe is its subatomic size, which can measure free volume elements as small as 0.2 nm (Goworek 2015). Furthermore, its short lifetime in polymers (~ 1–5 ns) allows the measurement of dynamic and transient free volume elements arising from polymer chain segmental motions. This is especially relevant for higher cell wall moisture contents (> 10%), where polymer mobility is enhanced due to a high degree of plasticization degree, and some regions of the

cell wall undergo glass transition (Jakes 2019). Beyond favorable length and time scales, PALS does not require specific sample preparation procedures like grinding or cutting into thin sections, thereby preserving the cell wall structure. Based on these advantages, PALS can potentially offer new information related to wood cell wall nanostructure that has so far not been possible with the commonly applied experimental techniques in the wood science community.

In this brief report, we present the first water-dependent PALS measurements performed on intact softwood cell walls. We describe our experimental approach, address data reproducibility, and provide an interpretation of the results. The discussion includes comparisons with previously published work using atomistic modeling and experimental methods, highlighting both similarities and differences in the data.

Materials and methods

Materials

Earlywood (EW) and latewood (LW) samples were extracted from the single growth ring of mature, compression-wood free loblolly pine (*P. taeda*), as utilized in a previous study (Arzola-Villegas 2022). The specimens were 10 mm in the longitudinal direction, 10 mm in the tangential direction, and 2 mm in the radial direction. The width and the length of the samples were chosen based on the designed sample holders, whereas the sample thickness was limited by the width of EW and LW bands within the growth ring. Based on the sample thickness (2 mm), density, and average implantation energy of positrons generated by ^{22}Na (0.215 MeV), it was estimated that approximately 99.9% of all positrons were stopped and annihilated in both EW and LW samples (calculation details can be found in Supplementary Information, S.1.).

The chemical composition and sorption isotherms of the samples originating from the same growth ring were previously published (Arzola-Villegas 2022). In summary, EW had approximately 3% higher lignin content than LW, while LW showed about 1% higher glucan and 2% higher mannan content. There were no observable differences between EW and LW equilibrium moisture contents between 0 and 95% relative humidity (RH). Samples were stored above silica gel (~ 1% RH) before PALS measurements.

Relative humidity equilibration

In-situ RH control was achieved using a custom-made sample chamber (chamber design details can be found in (Attallah et al. 2023)) in combination with silica gel or saturated salt solutions. Two identical samples, separated by a ^{22}Na positron source, were positioned in the center of the sample chamber, whereas the silica gel or saturated salt solution corresponding to a specific RH step was placed in the outer ring of the chamber. RH values within the sample chamber were measured using BME280 (Bosch, Gerlingen, Germany) humidity sensor with an RH accuracy tolerance of ± 3%. SiO_2, LiCl, $MgCl_2$, $Mg(NO_3)_2$, and NaCl were used to achieve RH ranges between ~ 1 and 80% RH. The samples were kept in the controlled climate for at least 24 h before initiating PALS measurement. This was estimated as sufficient time to achieve stable wood moisture content based on previous sorption studies of loblolly pine (Glass et al. 2018). Furthermore, statistical errors of o-Ps lifetimes and corresponding intensities were lower than 0.5 and 0.3% during data collection (Supplementary Information, S.6.), indicating free volume equilibrium. Time series of relative humidity data were continuously monitored throughout the experiments using InfluxDB (InfluxData, San Francisco, California).

It should be noted that measurements using $MgCl_2$, $Mg(NO_3)_2$, and NaCl resulted in discrepancies, including RH values not corresponding to theoretical values found in the literature and variations in RH values between different sample measurements using the same salt. These discrepancies were likely due to suboptimal airtightness of the developed sample chamber and/or its design, which limited the amount of saturated salt solution that could be placed within the chamber. Nonetheless, RH values stabilized after an equilibration period between the salt solution and the sample chamber environment. RH values for each sample and RH steps can be found in Supplementary Information (S.1).

Additionally, during the LW sample measurements using NaCl, the salt solution came into contact with

the positron source, necessitating the immediate termination of the experiment to avoid further contamination risks. As a result, the results associated with LW samples at the highest measured RH are not reported.

PALS measurements

PALS experiments were performed using a digitizer (Teledyne SP-Devices, ADQ14DC-2X-MTCA) with four photomultiplier tubes (Hamamatsu R13089, Model 265) coupled to cylindrical CeBr3 scintillators (5.08 cm diameter and 2.54 cm thickness) for detecting gamma radiation associated with positron annihilation. Prior to PALS measurements on wood samples, reference samples (Ti, Ta, Al) were used to determine the source contribution (i.e., positrons annihilating in the source material) and the instrument resolution function. These reference materials exhibit a single positron lifetime component in addition to the source components, resulting in constant values for both resolution function and source correction (Supplementary Information, S.3.) (Robles et al. 2007). While source components are commonly used as source correction in PALS analysis, we analyzed these components as part of the main lifetime components. We chose this approach due to discrepancies between the source correction method in PALSFit and the inclusion of two additional components in the normal fit. Mathematically, there should be no difference. The source correction for different RH levels was determined by individual reference measurements. At higher RH levels (above 40%), the long component becomes more dominant (with increased intensity), while the Kapton component remains constant. We opted to use the additional component approach to maintain full control over the source parameters for each RH step, as in the source correction method, the individual ratio could not be adapted.

Following the reference measurements, the EW and LW samples at specific RH were measured by placing a ^{22}Na positron source (source activity of 1.69 MBq), covered with a 5 µm *DuPont*™ *Kapton*® foil, between two EW or LW samples (described in Materials section). The assembled wood-source-wood sandwiches were subsequently placed in a PALS sample chamber together with the saturated salt solution. The reason for using two samples per measurement is to maximize the solid angle of sample material surrounding the positron source, thereby reducing the measurement time. The wood-source-wood sandwich was kept in the sample chamber for at least 24 h to allow wood cell walls to reach equilibrium moisture content. Afterward, PALS measurements were initiated, each lasting approximately 5 h to collect 5×10^6 positron annihilation events.

PALS spectra were analyzed by fitting the measured exponential decay curves to the recorded time differences histograms using the PALSFit routine (Olsen et al. 2007). More details regarding data analysis can be found in Supplementary Information (S.4.). The sizes of the cell wall free volume elements were based on recorded positron lifetimes (ns) using the general Tao-Eldrup model, which assumes a spherical shape for the free volume element (Supplementary Information, S.5.).

Results and discussion

Since positron annihilation adheres to the principles of radioactive decay, the measured PALS spectra represent the sum of different exponential decay

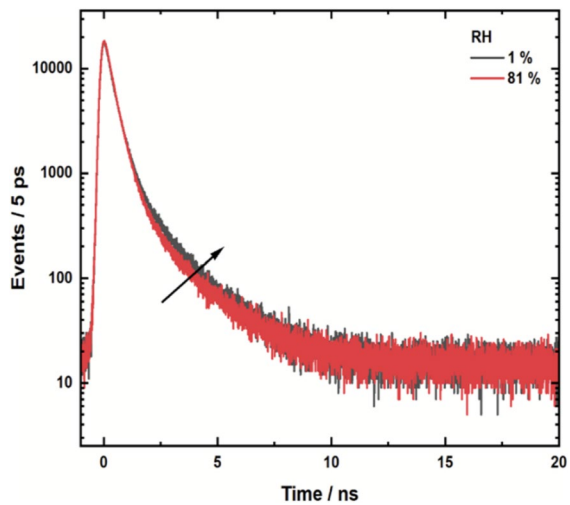

Fig. 2 Example of PALS spectra (EW 1–2 sample at 1% and 81% RH) convoluted with instrumental resolution function of the measurement system and subject to background noise. X-axis represents the time between the start signal of a positron and its annihilation signal with a shifted peak maximum at 0 ns. Y-axis represents the number of positron annihilation events (with 5 ps channel dispersion)

components, i.e., free positrons, p-Ps and o-Ps, each characterized by distinct lifetimes (reciprocals of the slopes of the decay curve) and intensities (areas under the component) (Fig. 2). Consequently, isolating the information related to the cell wall free volume (i.e., o-Ps lifetimes and intensities) requires deconvolution of the experimental decay curve into separate positron lifetime components.

The analysis of the experimental decay curve revealed five positron lifetime components (τ) for all samples and levels of RH (details in Supplementary Information, S.6.). Of these, the components τ_2 (0.382 ns) and τ_5 (2.52 ns) were attributed to the source correction (positrons annihilating in the 5 µm *DuPont*™ *Kapton*® foil covering the ^{22}Na source) and were fixed for the analysis (Supplementary Information, S.3.). The components τ_1 (0.269 and 0.247 ns for EW and LW, respectively) is attributed to a mixture of p-Ps annihilation events and annihilation in the wood bulk material. Separation of these two annihilation modes is not possible due to the resolution of the spectrometer. The component τ_3 (0.460 and 0.434 ns for EW and LW, respectively) was assigned to the annihilation of free positrons (e^+) and was fixed for the analysis together with τ_1 to reduce the variation in corresponding intensities. The lifetime component τ_4 (~1.6–1.9 ns depending on the RH), characteristic of o-Ps annihilation in the free volume elements of amorphous polymers (Hagiwara et al. 2000; Dlubek et al. 2004), was assigned to the free volume elements of amorphous cell wall polymer regions.

In semicrystalline polymers, an additional shorter τ component associated with o-Ps annihilation in the crystalline phase can sometimes be observed due to denser and more uniform chain packing, resulting in smaller free volume elements (Dlubek et al. 1998, 2002b). In wood cell walls, the regions of amorphous and crystalline cellulose, amorphous hemicelluloses, and lignin are also likely to exhibit distinct free volume characteristics. However, the presence of a single o-Ps component suggests that the differences in o-Ps lifetimes (free volume element sizes) between individual cell wall polymers are not large enough to resolve into multiple components. In other words, the lifetimes and corresponding intensities of the τ_4 component at specific RH levels represent mean values of all measured o-Ps annihilation events in the wood cell wall polymers. The o-Ps distribution measurement is possible by using MELT analysis (Zaleski 2006). However, this approach requires measuring a significantly higher number of annihilation events (i.e., higher statistics), which was not done in this preliminary study since our focus was on determining whether PALS could reproducibly measure humidity-dependent changes in the cell wall free volume. In future studies, MELT analysis could be performed to gain more insight into the distribution of the free volume of wood cell walls at equilibrium conditions.

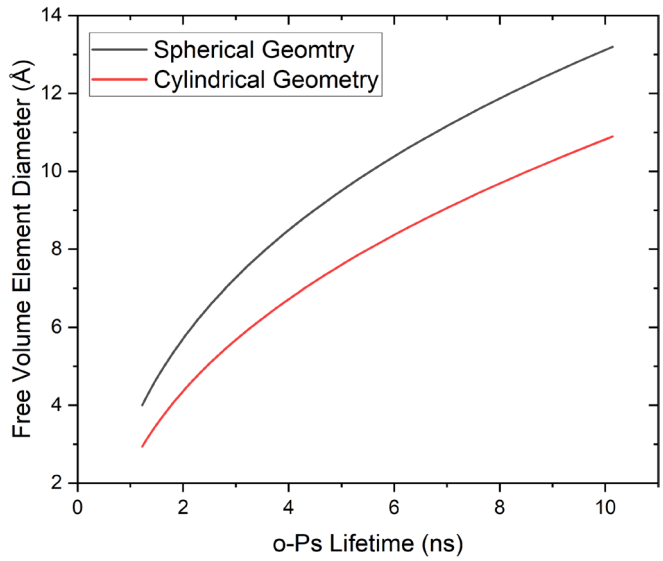

Fig. 3 Relationship between measured o-Ps lifetimes and spherical/cylindrical diameters of free volume elements obtained by Tao-Eldrup model. The red frame shows the values corresponding to measured o-Ps lifetimes in wood samples

Figure 3 shows the relationship between the measured o-Ps lifetimes and free volume element diameters based on the semi-empirical model proposed by Tao (Tao 1972) and Eldrup (Eldrup et al. 1981). In short, the model assumes that the o-Ps resides in a simple infinite potential well (in this case, a spherical well with radius *r)* (calculation details in Supplementary Information, S.5.). Although the free volume elements of amorphous polymers are realistically characterized by irregular geometrical shapes, the spherical shape assumption has been widely adopted due to its simplicity (Goworek et al. 1997; Śniegocka et al. 2005) and is also included here for comparison to spherical diameters measured by PALS in other polymers.

The calculated free volume spherical diameter values for wood samples (~5.4–6.0 Å depending on the RH level) are approximately 15–35% higher than those reported in the PALS literature discussing swelling of the polysaccharide matrices (Edlund et al. 2012; Roussenova and Alam 2013; Torstensen et al. 2018). This discrepancy may result from a more heterogeneous structural arrangement of the cell wall polymers, including polymer–polymer interfaces and interphases characterized by lower chain packing density. Furthermore, similar values were found in a PALS study investigating the moisture-induced plasticization of polyvinyl alcohol (spherical diameters of approximately 4 and 5.5 Å for dry and water-saturated state, respectively) (Hodge et al. 1996), which is structurally much simpler than the wood cell wall. Comparable values were also measured in pine by Li and Zhao (Li and Zhao 2020) using moisture-dependent time-domain nuclear magnetic resonance to evaluate cell wall porosity, although the pore sizes were only affected above ~ 70% RH. These authors also reported ~ 2.2 times higher average cell wall pore sizes in poplar than in pine, suggesting that the free volume might be significantly influenced by variations in cell wall polymer structures and their relative amounts in different wood species.

Free volume elements in wood cell walls, sometimes referred to as micropores or nanopores in wood science literature, have also been assumed to be cylindrical in shape (Shi and Avramidis 2017). Therefore, cylindrical diameters of the free volume elements calculated from the adapted Tao-Eldrup equation (Olson et al. 2002) are also plotted in Fig. 3.

The calculated cylindrical diameters are smaller than the spherical values, but this depends on the assumed cylinder length (here L = 2R was assumed) (Olson et al. 2002). Whether spherical or cylindrical models are more applicable for free volume elements in lignocellulosic materials like wood remains uncertain. However, they are the two most likely geometries, and both are included here for potential comparisons in future PALS experiments.

In addition to providing information related to the polymer free volume, PALS can also detect larger voids up to approximately 100 nm in diameter. In voids above this size, the o-Ps lifetime approaches that of annihilation in vacuum (142 ns) and, hence, cannot provide useful information related to material structure anymore. Based on this, one would expect the presence of additional o-Ps components related to voids other than polymer free volume (e.g., meso- and macropores) under ~ 100 nm to be present in the PALS spectra. The absence of additional o-Ps components annihilating in larger voids is in contradiction with numerous gas adsorption (Kojiro et al. 2010; Yin et al. 2015; Shi and Avramidis 2018) and NMR-based cryoporometry (Gao, X., Zhuang, S., Jin, J., and Cao, P. 2015; Cao et al. 2021) studies performed on wood. While these studies report the presence of voids as large as 30 nm in the wood cell wall structure, a recent study suggests these results likely originate from methodological issues (Nopens et al. 2020). Furthermore, inadequate sample preparation approaches (e.g., wood milling) have been shown to introduce additional porosity not present in the native wood cell walls (Zelinka et al. 2012). From this perspective, the advantage of PALS lies in the high initial kinetic energy of generated positrons, resulting in o-Ps annihilation in the bulk of the wood samples. In other words, the cell walls on the sample surface, which may have been damaged during sample preparation, are not probed.

One of the main advantages of PALS is the ability to probe the polymer free volume in a controlled climate. The evolution of o-Ps lifetimes (τ_4), corresponding free volume element sizes, and intensities (Int_4) of EW and LW samples with RH is shown in Fig. 4. Since two identical wood samples were used in PALS measurements, the numbers in the legend, i.e., 1–2 or 3–4, correspond to these samples. To demonstrate the reproducibility of measured data,

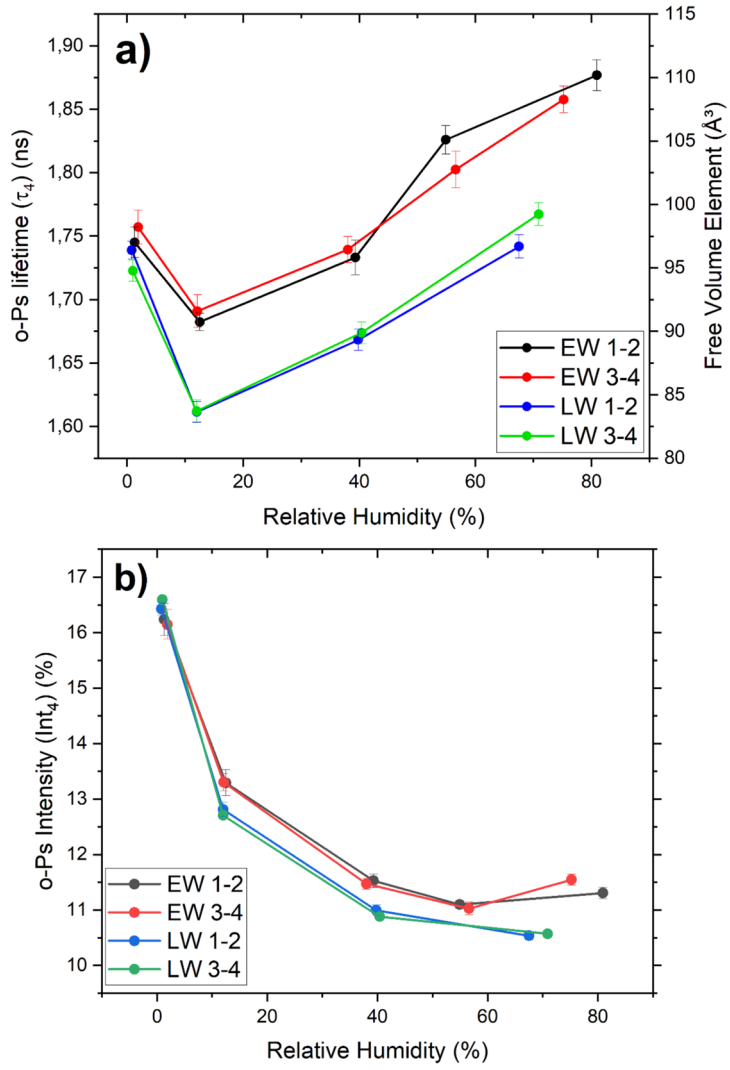

Fig. 4 Mean o-Ps lifetimes (τ4) and free volume element sizes (derived from Tao-Eldrup model) (a), and mean o-Ps intensities (Int4) (b). The error bars represent standard errors

both sample sets for EW and LW have been plotted individually on the graph. Figure 4a illustrates that τ4 and corresponding free volume element sizes (right axis) are consistent between the two sample sets at each RH level. Similarly, Fig. 4b shows that the o-Ps intensities show comparable values for both EW and LW samples across all tested RH levels, underscoring good data reproducibility of PALS.

We will first discuss the data related to o-Ps lifetimes (τ4) and corresponding free volume element sizes (Figure 4a) calculated via the Tao-Eldrup model. The first observation that can be made is the sharp decrease of the free volume element sizes occurring between ~ 1 and 11% RH. The initial decrease of the polymer free volume at low RH, also known as antiplasticization, due to water absorption has already been extensively discussed in polymer science literature (Guo 1993; Dlubek et al. 2002a; Kilburn et al. 2005; Roussenova et al. 2010). While there is no clear consensus regarding the exact mechanisms responsible for water-induced antiplasticization, it is most often interpreted in terms of strong hydrogen bonding interactions between polymer functional groups and water, which lead to partial filling of the free volume elements present in the dry polymer matrix. Considering the volume of a water molecule in liquid water (30 $Å^3$) and the estimated mean free volume sizes of dry EW and LW cell walls (94–98 $Å^3$), the mechanism of free volume filling by water molecules can certainly be envisaged. Our data

provides experimental evidence to previous simulation-based studies speculating the decrease of cell wall porosity due to initial water sorption (Kulasinski et al. 2015; Shi and Avramidis 2019). Furthermore, antiplasticization can likely explain the commonly observed increase in wood mechanical properties (Gerhards 1982; Obataya et al. 1998; Youssefian et al. 2017) and swelling lag (Mantanis et al. 1994) at low wood moisture contents (< 5%).

While there is no significant difference in the free volume element sizes of EW and LW samples at dry conditions, the initial antiplasticization-induced decrease in free volume is more pronounced in LW samples. Given that the chemical composition and cell wall moisture content at a given RH are similar for EW and LW samples (Arzola-Villegas 2022), the observed differences in τ_4 at low RH likely stem from variations in the free volume characteristics inherent to EW and LW cell walls. However, assuming o-Ps annihilations are evenly distributed within the amorphous polymer matrix of the cell walls, identifying the exact cell wall regions associated with the differences in τ_4 between EW and LW is difficult. One potential explanation could be related to the differences in the thickness of individual cell wall layers in EW and LW. Specifically, it has been reported that the LW of loblolly pine has a significantly thicker S2 layer (80% of the overall cell wall material fraction) compared to EW (Saka, S, RJ Thomas, and JS Gratzl 1981). Conversely, EW has a thinner S2 layer (comprising 60% of the overall cell wall material fraction) and thicker S1, S3, and compound middle lamella layers. As a consequence of the differing relative volume fractions of individual cell wall layers, and hence minor chemical composition differences as described in the Materials section, it is possible that the relative amount of free volume elements in dry EW and LW cell walls contributing to antiplasticization during initial water absorption differ.

After the initial antiplasticization stage, water starts to act as a plasticizer, i.e., polymer chain segments gain mobility, and the mean free volume element sizes increase. As a result of the initial antiplasticization stage, the mean free volume element sizes of EW remain higher than those of LW at all subsequent RH levels above 11%. However, there are no clearly observable differences in trends between both sample types during this stage. Interestingly, it takes a significant amount of water acting as a plasticizer to recover the mean free volume element size (i.e., volume not occupied by polymers and water) that was initially lost during the antiplasticization. Specifically, the mean free volume element sizes reach those of dry cell walls at approximately 40 and 60% RH for EW and LW, respectively. These RH levels correspond to 8–11% moisture content (Arzola-Villegas 2022), which is well above the low moisture contents (< 5%) in which a lag in bulk swelling is observed. This indicates that bulk swelling in wood is not directly proportional to just the measured mean free volume element sizes. Swelling is expected to also depend on the number of free volume elements and the volume of the absorbed water molecules.

Another notable observation is the τ_4 of EW samples reaching ~ 1.85 ns at approximately 70% RH, corresponding to the o-Ps lifetime observed in liquid water at 20 °C (Kotera et al. 2005). This implies that 1) water molecules within cell walls behave similarly to liquid water at higher cell wall moisture contents, likely forming clusters, 2) the cell wall moisture content at which free volume is predominantly filled by water is lower for EW than LW, and 3) the o-Ps lifetime of ~ 1.85 ns cannot reliably estimate free volume element sizes due to overlap with the o-Ps lifetime of water. The last point was confirmed by an additional PALS experiment conducted on LW samples during desorption at 95, 85 and 75% RH, starting from water-saturated sample states (Supplementary Information, S.2). In each case, τ_4 was approximately 1.85 ns, i.e., the majority of the measured o-Ps annihilations originated from liquid-like water.

The intensity of o-Ps (*Int*) (Fig. 4b) is a measure of how many positrons form o-Ps and undergo annihilation in the material. Therefore, it is commonly used to estimate the relative number of free volume elements in polymers (Kobayashi et al. 1989). That being said, the interpretation of *Int* becomes more complicated in the presence of water within materials, as it has been shown to inhibit o-Ps formation (Ito and Tabata 1972; Jean et al. 2003). This can be explained by considering the solvation of o-Ps precursors (i.e., free positrons and electrons) by clusters of water molecules. In polymers, *Int* is typically observed to decrease with increasing concentration of water in the matrix, which has also been discussed from the perspective of water-induced inhibition of o-Ps formation (Ito et al. 1993; Sánchez et al. 1995; Dlubek et al. 1999).

In our study, Int_4 is observed to decrease exponentially, eventually leveling off at approximately 60% RH. During the initial antiplasticization stage, a more pronounced reduction in Int_4 is observed. While o-Ps inhibition possibly contributes to the Int_4 reduction, it is also important to consider that water molecules mostly fill the free volume elements at this stage of water absorption, thereby reducing the sizes and possibly the numbers of free volume elements. This reduction in free volume likely contributes more significantly to the observed decrease in Int_4, as water clustering, which is mainly responsible for o-Ps inhibition, is not expected to be substantial at such low water concentrations (Sánchez et al. 1995). The more pronounced decrease in Int_4 observed for LW compared to EW suggests that LW has a higher proportion of free volume elements susceptible to water filling (i.e., antiplasticization), which aligns with the observations previously made for τ_4 (Fig. 4a).

During the plasticization stage of water absorption, segmental motions of polymer chains are facilitated, resulting in an increase in the polymer's free volume. From this perspective, one might initially expect that a further reduction in Int_4 during cell wall plasticization indicates the merging of individual free volume elements, leading to fewer o-Ps localization spots. However, o-Ps inhibition is also anticipated to become more dominant as the cell wall moisture content increases due to gradually increasing water cluster sizes (Kulasinski et al. 2014). It is likely that both mechanisms take place simultaneously, further complicating the interpretation. The eventual stabilization of Int_4 around 60% RH indicates that all voids within the cell walls are predominantly saturated with water, leading to no further reduction in o-Ps formation probability. This observation aligns with previous findings for τ_4, suggesting that the majority of o-Ps annihilate in water clusters at high RH.

Conclusion

In this work, we explored the applicability of positron annihilation lifetime spectroscopy (PALS) to study the water-dependent free volume properties of wood cell walls. The data collected for earlywood and latewood samples of loblolly pine has shown reproducibility at all measured relative humidities (RH) and aligned with polymer science principles. Specifically, water can act as both an antiplasticizer (decreasing free volume below 11% RH) and a plasticizer (increasing free volume above 11% RH) in wood cell walls. Although no observable differences were found between free volume characteristics of dry earlywood and latewood cell walls, latewood exhibited a more substantial decrease in free volume element sizes during the initial stage of water absorption, suggesting a higher degree of antiplasticization. At higher RH levels, the ortho-positronium lifetimes (indicative of free volume element sizes) in earlywood overlapped with those measured in liquid water, indicating that the majority of the voids within cell walls were occupied by water clusters. The possibility of water clusters inhibiting ortho-positronium formation in the cell wall free volume complicated the interpretation of ortho-positronium annihilation intensities.

Acknowledgements We thank Andreas Hartmann and Daniel Stach from HZDR for their dedicated contributions to preparing and commissioning the PALS humidity chamber.

Author Contributions F.M. and E.H. conecptualized the study. J.E.J prepared the wood samples. Data collection was performed by E.H. Data analysis was performed by E.H. and F.M. Original draft was prepared by F.M. Further review and editing of the manuscript was done by F.M., E.H., M.B., A.G.A, and J.E.J. Resources and supervision was provided by A.W.

Funding Open Access funding enabled and organized by Projekt DEAL. The research was funded by the InnoRenew project (Grant Agreement #739574) under the Horizon2020 Widespread-Teaming program and the Republic of Slovenia (Investment funding of the Republic of Slovenia and the European Regional Development Fund).

Data availability Data is provided within the manuscript and supplementary information files. Additional raw data can be provided by the corresponding author upon reasonable request.

Declarations

Conflict of Interests The authors declare no competing interests.

References

Arzola-Villegas X, Lakes R, Plaza NZ, Jakes JE (2019) Wood moisture-induced swelling at the cellular scale—Ab intra. Forests 10(11):996. https://doi.org/10.3390/f10110996

Arzola-Villegas (2022) Micro-X-ray Computed Tomography Study of Moisture Swelling in Wood Cell Walls and Cellular Structures. Dissertation, University of Wisconsin

Attallah AG, Bon V, Maity K, Hirschmann E, Butterling M, Wagner A, Kaskel S (2023) Unravelling the water adsorption mechanism in hierarchical MOFs: insights from in situ positron annihilation lifetime studies. ACS Appl Mater Interfaces 15(41):48264–48276. https://doi.org/10.1021/acsami.3c10974

Cao H, Lyu J, Zhou Y (2021) Gao X the study of bound water status and pore size distribution of chinese fir and poplar cell wall by low-field NMR. Int J Polym Sci 4954837:11. https://doi.org/10.1155/2021/4954837

Chen M, Coasne B, Guyer R, Derome D, Carmeliet J (2018) Role of hydrogen bonding in hysteresis observed in sorption-induced swelling of soft nanoporous polymers. Nat Commun 9(1):3507. https://doi.org/10.1038/s41467-018-05897-9

De Yao K, Liu J, Zhao RZ, Wang WH, Wei L (1998) Dynamic water absorption characteristics of chitosan-based hydrogels an investigation by positron annihilation lifetime spectroscopy. Die Angew Makromol Chemie. 255(1):71–75

Dlubek G, Saarinen K, Fretwell HM (1998) The temperature dependence of the local free volume in polyethylene and polytetrafluoroethylene: a positron lifetime study. J Polym Sci, Part b: Polym Phys 36(9):1513–1528. https://doi.org/10.1002/(SICI)1099-0488(19980715)36:9%3c1513::AID-POLB9%3e3.0.CO;2-K

Dlubek G, Buchhold R, Hübner Ch, Nakladal A (1999) Water in local free volumes of polyimides: a positron lifetime study. Macromolecules 32(7):2348–2355. https://doi.org/10.1021/ma981381s

Dlubek G, Redmann F, Krause-Rehberg R (2002a) Humidity-induced plasticization and antiplasticization of polyamide 6: a positron lifetime study of the local free volume. J Appl Polym Sci 84(2):244–255. https://doi.org/10.1002/app.10319

Dlubek G, Stejny J, Lüpke Th, Bamford D, Petters K, Hübner Ch, Alam MA, Hill MJ (2002b) Free-volume variation in polyethylenes of different crystallinities: positron lifetime, density, and X-ray studies. J Polym Sci, Part b: Polym Phys 40(1):65–81. https://doi.org/10.1002/polb.10072

Dlubek G, Kilburn D, Bondarenko V, Pionteck J, Krause-Rehberg R, Alam MA (2004) Positron annihilation: a unique method for studying polymers. Macromol Symp 210(1):11–20. https://doi.org/10.1002/masy.200450602

Edlund U, Yu Y, Zhu Ryberg Y, Krause-Rehberg R, Albertsson A-C (2012) Positron lifetime reveals the nano level packing in complex polysaccharide-rich hydrolysate matrixes. Anal Chem 84(8):3676–3681. https://doi.org/10.1021/ac300152g

Eldrup M, Lightbody D, Sherwood JN (1981) The temperature dependence of positron lifetimes in solid pivalic acid. Chem Phys 63(1):51–58. https://doi.org/10.1016/0301-0104(81)80307-2

Fukuzumi H, Saito T, Iwamoto S, Kumamoto Y, Ohdaira T, Suzuki R, Isogai A (2011) Pore size determination of TEMPO-oxidized cellulose nanofibril films by positron annihilation lifetime spectroscopy. Biomacromol 12(11):4057–4062. https://doi.org/10.1021/bm201079n

Gao X, Zhuang S, Jin J, Cao P (2015) Bound water content and pore size distribution in swollen cell walls determined by NMR technology. Bioresources 10(4):8208–8224

Gerhards CC (1982) Effect of Moisture Content and Temperature on the Mechanical Properties of Wood: An Analysis of Immediate Effects. Wood and Fiber Number 1(January 1982):4–36

Glass SV, Boardman CR, Thybring EE, Zelinka SL (2018) Quantifying and reducing errors in equilibrium moisture content measurements with dynamic vapor sorption (DVS) experiments. Wood Sci Technol 52(4):909–927. https://doi.org/10.1007/s00226-018-1007-0

Glass SV, Zelinka SL (2010) Moisture relations and physical properties of wood. Wood handbook : wood as an engineering material: chapter 4 Centennial ed General technical report FPL ; GTR-190 Madison, WI : US Dept of Agriculture, Forest Service, Forest Products Laboratory, 2010: p 41–419 190:4.1–4.19

Goworek T (2015) Positronium as a probe of small free volumes in crystals, polymers and porous media. Annales Universitatis Mariae Curie-Sklodowska sectio AA–Chemia. https://doi.org/10.2478/umcschem-2013-0012

Goworek T, Ciesielski K, Jasińska B, Wawryszczuk J (1997) Positronium in large voids. Silicagel Chem Phys Letters 272(1):91–95. https://doi.org/10.1016/S0009-2614(97)00504-6

Guo J-H (1993) Effects of plasticizers on water permeation and mechanical properties of cellulose acetate: antiplasticization in slightly plasticized polymer film. Drug Dev Ind Pharm 19(13):1541–1555. https://doi.org/10.3109/03639049309069325

Hagiwara K, Ougizawa T, Inoue T, Hirata K, Kobayashi Y (2000) Studies on the free volume and the volume expansion behavior of amorphous polymers. Radiat Phys Chem 58(5):525–530. https://doi.org/10.1016/S0969-806X(00)00211-5

Hautojärvi P (2012) Positrons in Solids. Springer Science & Business Media

Hodge RM, Bastow TJ, Edward GH, Simon GP, Hill AJ (1996) Free volume and the mechanism of plasticization in water-swollen poly(vinyl alcohol). Macromolecules 29(25):8137–8143. https://doi.org/10.1021/ma951073j

Hunt C, Frihart C, Dunky M, Rohumaa A (2018) Understanding wood bonds-going beyond what meets the eye: a critical review. Rev Adhes Adhes 6:369–463. https://doi.org/10.7569/RAA.2018.097312

Ito Y, Tabata Y (1972) The intensity of ortho-positronium component in liquid and solid amides. Chem Phys Lett 15(4):584–585. https://doi.org/10.1016/0009-2614(72)80377-4

Ito Y, Sanchez V, Lopez R, Fucugauchi LA, Tanaka K, Okamoto K (1993) The effects of vapor sorption in polymers observed by positron annihilation. Bull Chem Soc Jpn 66(3):727–732. https://doi.org/10.1246/bcsj.66.727

Jakes JE (2019) Mechanism for diffusion through secondary cell walls in lignocellulosic biomass. J Phys Chem B 123(19):4333–4339. https://doi.org/10.1021/acs.jpcb.9b01430

Jakes JE, Hunt CG, Zelinka SL, Ciesielski PN, Plaza NZ (2019) Effects of moisture on diffusion in unmodified wood cell walls: a phenomenological polymer science approach. Forests 10(12):1084. https://doi.org/10.3390/f10121084

Jean YC, Mallon PE, Schrader DM (2003) Principles and Applications of Positron & Positronium Chemistry. World Scientific

Jean YC, Van Horn JD, Hung W-S, Lee K-R (2013) Perspective of positron annihilation spectroscopy in polymers. Macromolecules 46(18):7133–7145. https://doi.org/10.1021/ma401309x

Kilburn D, Claude J, Schweizer T, Alam A, Ubbink J (2005) Carbohydrate polymers in amorphous states: an integrated thermodynamic and nanostructural investigation. Biomacromol 6(2):864–879. https://doi.org/10.1021/bm049355r

Kobayashi Y, Zheng W, Meyer EF, McGervey JD, Jamieson AM, Simha R (1989) Free volume and physical aging of poly(vinyl acetate) studied by positron annihilation. Macromolecules 22(5):2302–2306. https://doi.org/10.1021/ma00195a052

Kojiro K, Miki T, Sugimoto H, Nakajima M, Kanayama K (2010) Micropores and mesopores in the cell wall of dry wood. J Wood Sci 56(2):107–111. https://doi.org/10.1007/s10086-009-1063-z

Kotera K, Saito T, Yamanaka T (2005) Measurement of positron lifetime to probe the mixed molecular states of liquid water. Phys Lett A 345(1):184–190. https://doi.org/10.1016/j.physleta.2005.07.018

Kulasinski K, Guyer RA (2016) Quantification of nanopore networks: application to amorphous polymers. J Phys Chem C 120(49):28144–28151. https://doi.org/10.1021/acs.jpcc.6b10777

Kulasinski K, Keten S, Churakov SV, Guyer R, Carmeliet J, Derome D (2014) Molecular mechanism of moisture-induced transition in amorphous cellulose. ACS Macro Lett 3(10):1037–1040. https://doi.org/10.1021/mz500528m

Kulasinski K, Guyer R, Derome D, Carmeliet J (2015) Water adsorption in wood microfibril-hemicellulose system: role of the crystalline-amorphous interface. Biomacromol 16(9):2972–2978. https://doi.org/10.1021/acs.biomac.5b00878

Lenth CA (2001) Kamke FA (2001) moisture dependent softening behavior of wood. Wood and Fiber Science Number 3:492–507

Li X, Zhao Z (2020) Time domain-NMR studies of average pore size of wood cell walls during drying and moisture adsorption. Wood Sci Technol 54(5):1241–1251. https://doi.org/10.1007/s00226-020-01209-x

Mantanis GI, Young RA, Rowell RM (1994) Swelling of wood: part 1. swelling in water. Wood sci techn 28:119–134

Nopens M, Sazama U, König S, Kaschuro S, Krause A, Fröba M (2020) Determination of mesopores in the wood cell wall at dry and wet state. Sci Rep 10(1):9543. https://doi.org/10.1038/s41598-020-65066-1

Obataya E, Norimoto M, Gril J (1998) The effects of adsorbed water on dynamic mechanical properties of wood. Polymer 39(14):3059–3064. https://doi.org/10.1016/S0032-3861(97)10040-4

Olsen JV, Kirkegaard P, Pedersen NJ, Eldrup M (2007) PALSfit A new program for the evaluation of positron lifetime spectra. Phys Status Solidi c. 4(10):4004–4006

Olson BG, Prodpran T, Jamieson AM, Nazarenko S (2002) Positron annihilation in syndiotactic polystyrene containing α and β crystalline forms. Polymer 43(25):6775–6784. https://doi.org/10.1016/S0032-3861(02)00604-3

Resch L, Karner A, Sprengel W, Würschum R, Schennach R (2022) Water intake of cellulose materials monitored by positron annihilation lifetime spectroscopy. Cellulose 29(3):1357–1363. https://doi.org/10.1007/s10570-021-04367-8

Robles JMC, Ogando E, Plazaola F (2007) Positron lifetime calculation for the elements of the periodic table. J Phys: Condens Matter 19(17):176222. https://doi.org/10.1088/0953-8984/19/17/176222

Roussenova M, Alam MA (2013) PALS: A unique probe for the molecular organisation of biopolymer matrices. J Phys: Conf Ser 443(1):012044. https://doi.org/10.1088/1742-6596/443/1/012044

Roussenova M, Murith M, Alam A, Ubbink J (2010) Plasticization, antiplasticization, and molecular packing in amorphous carbohydrate-glycerol matrices. Biomacromol 11(12):3237–3247. https://doi.org/10.1021/bm1005068

Rowell R, Pettersen R, Han J, Rowell J, Tshabalala M (2012) Cell Wall Chemistry. In: Handbook of Wood Chemistry and Wood Composites, Second Edition. CRC Press

Ruark AE (1945) Positronium. Phys Rev 68(11–12):278–278. https://doi.org/10.1103/PhysRev.68.278

Saka, S, RJ Thomas, and JS Gratzl (1981) Lignin distribution in Douglas-fir and loblolly pine as determined by energy dispersive X-ray analysis. In: International Symposium on Wood and Pulping Chemistry. SPCI, Stockholm, pp 29–37

Sánchez V, López R, Fucugauchi LA, Ito Y (1995) Positron annihilation lifetime study of vapor sorption in polypropylene and polytetrafluoroethylene. J Appl Polym Sci 56(7):779–791. https://doi.org/10.1002/app.1995.070560703

Schrader DM, Jean YC (1988) Positron and Positronium Chemistry. Elsevier

Sharma SK, Pujari PK (2017) Role of free volume characteristics of polymer matrix in bulk physical properties of polymer nanocomposites: a review of positron annihilation lifetime studies. Prog Polym Sci 75:31–47. https://doi.org/10.1016/j.progpolymsci.2017.07.001

Sharma SK, Zaydouri A, Roudaut G, Duplâtre G (2011) Effect of water on glass transition in starch/sucrose matrices investigated through positron annihilation lifetime spectroscopy: a new approach. Phys Chem Chem Phys

13(43):19338–19344. https://doi.org/10.1039/C1CP21243E
Shi J, Avramidis S (2017) Water sorption hysteresis in wood: III physical modeling by molecular simulation. Holzforschung 71(9):733–741. https://doi.org/10.1515/hf-2016-0231
Shi J, Avramidis S (2018) Dried cell wall nanopore configuration of douglas-fir, western red cedar and aspen heartwoods. Wood Sci Technol 52(4):1025–1037. https://doi.org/10.1007/s00226-018-1011-4
Shi J, Avramidis S (2019) Evolution of wood cell wall nanopore size distribution in the hygroscopic range. Holzforschung 73(10):899–910. https://doi.org/10.1515/hf-2018-0198
Śniegocka M, Jasińska B, Wawryszczuk J, Zaleski R, Deryło-Marczewska A, Skrzypek I (2005) Testing the extended tao-eldrup model silica gels produced with polymer template. Acta Physica Polonica A. 107(5):868–873
Suzuki H, Azami K, Komagata S, Kanazawa I, Suzuki R, Ohdaira T (2010) Diffusion of positrons in polymers studied by slow positron beam. J Phys: Conf Ser 225(1):012053. https://doi.org/10.1088/1742-6596/225/1/012053
Tao SJ (1972) Positronium annihilation in molecular substances. J Chem Phys 56(11):5499–5510
Terashima N, Kitano K, Kojima M, Yoshida M, Yamamoto H, Westermark U (2009) Nanostructural assembly of cellulose, hemicellulose, and lignin in the middle layer of secondary wall of ginkgo tracheid. J Wood Sci 55(6):409–416. https://doi.org/10.1007/s10086-009-1049-x
Thybring EE, Glass SV, Zelinka SL (2019) Kinetics of water vapor sorption in wood cell walls: state of the art and research needs. Forests 10(8):704. https://doi.org/10.3390/f10080704
Torstensen JØ, Liu M, Jin S-A, Deng L, Hawari AI, Syverud K, Spontak RJ, Gregersen ØW (2018) Swelling and free-volume characteristics of TEMPO-oxidized cellulose nanofibril films. Biomacromol 19(3):1016–1025. https://doi.org/10.1021/acs.biomac.7b01814
Wiedenhoeft A, Miller R (2005) Structure and Function of Wood. In: Handbook of Wood Chemistry and Wood Composites. CRC Press
Yin J, Song K, Lu Y, Zhao G, Yin Y (2015) Comparison of changes in micropores and mesopores in the wood cell walls of sapwood and heartwood. Wood Sci Technol 49(5):987–1001. https://doi.org/10.1007/s00226-015-0741-9
Youssefian S, Jakes JE, Rahbar N (2017) Variation of nanostructures, molecular interactions, and anisotropic elastic moduli of lignocellulosic cell walls with moisture. Sci Rep 7(1):2054. https://doi.org/10.1038/s41598-017-02288-w
Zaleski R (2006) Measurement and analysis of the positron annihilation lifetime spectra for mesoporous silica. Acta Phys Pol, A 110(5):729–738
Zelinka SL, Lambrecht MJ, Glass SV, Wiedenhoeft AC, Yelle DJ (2012) Examination of water phase transitions in Loblolly pine and cell wall components by differential scanning calorimetry. Thermochim Acta 533:39–45. https://doi.org/10.1016/j.tca.2012.01.015
Zgardzińska B, Goworek T (2013) Positrons in cyclohexane. photoionization of positronium in solid phase? Chem Phys 421:10–14. https://doi.org/10.1016/j.chemphys.2013.05.011
Zhang C, Chen M, Keten S, Coasne B, Derome D, Carmeliet J (2021) Hygromechanical mechanisms of wood cell wall revealed by molecular modeling and mixture rule analysis. Sci Adv. https://doi.org/10.1126/sciadv.abi8919

Supporting Information

Positrons as Microprobes to Study Water-Dependent Free Volume of Wood Cell Walls: A Preliminary Study

Journal: *Cellulose*

Author list

Corresponding Author: Filip Majstorović
E-Mail: filip.majstorovic@wki.fraunhofer.de

Filip Majstorović [1,2], Eric Hirschmann [3], Maik Butterling [3], Ahmed G. Attallah [3,4], Andreas Wagner [3], Joseph E. Jakes [5]*

[1] Fraunhofer Institute for Wood Research, Wilhelm-Klauditz-Institut WKI, 38108 Braunschweig, Germany
[2] Faculty of Mathematics, Natural Sciences and Information Technologies, University of Primorska, 6000 Koper, Slovenia
[3] Institute of Radiation Physics, Helmholtz-Zentrum Dresden-Rossendorf, 01328 Dresden, Germany
[4] Physics Department, Faculty of Science, Minia University, Egypt
[5] Forest Biopolymers Science and Engineering, USDA Forest Service, Forest Products Laboratory, One Gifford Pinchot Drive, Madison, WI 53726, USA

S.1. Calculation of the minimum sample thickness

Positrons lose their kinetic energy through various processes involving atomic nuclei, plasmons, and phonons on their way into the material. In order to describe the penetration depth or implantation profile of these processes for source-based experiments, an implantation model for positrons from radioisotopes was developed based on empirical experiments on electrons (Brandt and Paulin 1977). Based on this, the following equation can be applied to calculate the appropriate sample thickness for PALS measurements:

$$z = \ln\left(\frac{1}{1-P}\right)\frac{E_{avg}{}^{\gamma}}{C_{+}Z^{\beta}\rho} \qquad (1)$$

z - Implantation depth in cm

P - Probably of residence

E_{avg} – Average implantation energy in MeV

Z - Atomic number

ρ - Density in g cm^{-3}

C_{+}, γ, β - Empirical parameters (C_{+}=12.6, γ=1.28, β=0.17)

The formula above was used to calculate the probability of positron residence in the sample (P) based on the sample thickness (0.2 cm) of EW and LW samples. For all samples, carbon was taken as a representative atom of wood structure (Z=6). ρ values of 0.3 and 0.8 g cm^{-3} were taken for EW and LW, respectively. These values were based on minimum density values observed in the sample batch. Average implantation energy (E_{avg}) of positrons was 0.215 MeV based on the Na-22 positron source used in the PALS experiment (Chong et al. 2019).

Based on the above parameters, the sample thickness of both EW and LW samples was sufficient to stop 99.9% of the positrons during PALS measurements.

S.2. Relative Humidity During PALS Measurements

Table 1 and Figure 1 below show RH values with standard deviations (in parentheses) associated with sample equilibration times and subsequent PALS measurement.

Table S.1 RH values during PALS measurements

Sample	SiO_2	LiCl	$MgCl_2$	$Mg(NO_3)_2$	NaCl
EW 1-2	1.3 (0.3)	12.5 (0.5)	39.3 (0.3)	54.9 (2.6)	80.9 (1.1)
EW 3-4	1.9 (0.5)	12.1 (0.1)	38 (2.4)	56.6 (1.6)	75.2 (1.2)
LW 1-2	0.8 (0.2)	12.0 (0.1)	39.8 (1.4)	67.5 (1.9)	/
LW 3-4	1.0 (0.2)	12.0 (0.1)	40.4 (1.4)	70.9 (1.3)	/

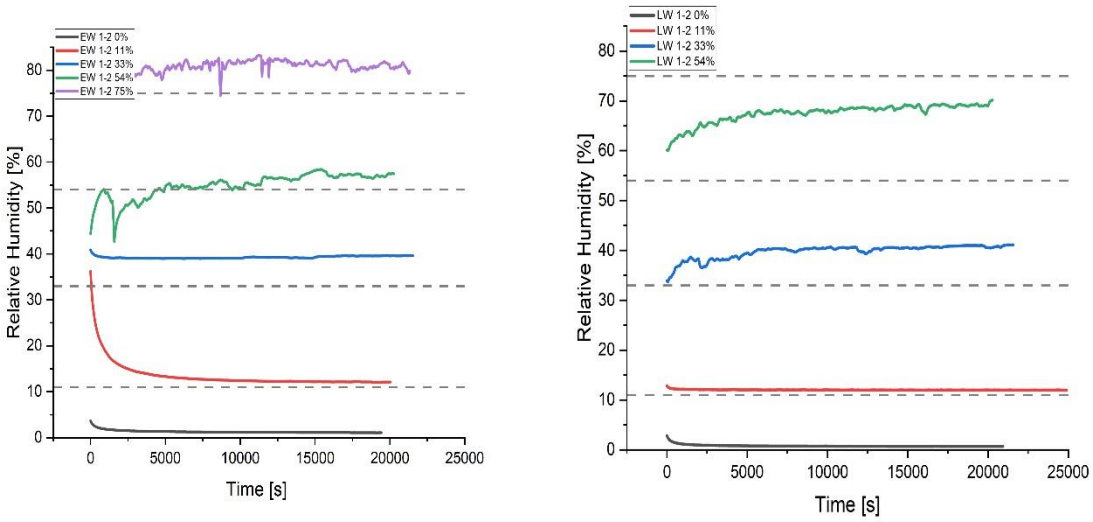

Fig S.1 *Relative humidity values during PALS measurements for EW (left) and LW (right) samples. Dashed lines represent the theoretical RH values corresponding to different saturated salt solutions.*

S.3. Reference Materials for PALS Measurements

In order to obtain a well-founded determination of the resolution function and source correction, various reference materials were investigated. These have the property that only one lifetime component is measured in addition to the source components. Consequently, for all reference materials, both the resolution function and the source correction should assume a constant value, since these have not been changed, see Table S.2. The reference materials used can be found in Table S.3.

Table S.2. Analysis parameters

$FWHM^{G}_1$	I^{G}_1	μ^{G}_1	$FWHM^{G}_2$	I^{G}_2	μ^{G}_2	τ^{SC}_1	τ^{SC}_2
231 ps	90%	0 ps	400 ps	10 %	-10 ps	382 ps	2520 ps

*Full width at half maxima (FWHM), Gaussian function (G), Source correction (SC)

Description	**Value**
Background range	900 to 1900 ns
Fit range	-3 to 34 ns

Under this condition, the values from Table S.3. could be determined. These show sufficient accuracy to the literature values.

Table S.3. Reference materials

Name	Symbol	Z	Density (cm^{-3})	τ^{Exp} (ps)	τ^{Lit} (ps)	I^{SC} (%)
Aluminium	Al	13	2.7	165	165	11.4
Titanium	Ti	22	4.5	148	147	11.5
Tantalum	Ta	73	16.7	121	120	15.6

Z – atomic number

τ^{Exp} – experimentally determined positron lifetime

τ^{Lit} – literature positron lifetimes (Robles et al. 2007)

I^{SC} – source correction intensity

S.4. PALS Analysis

In PALS experiment, the measured positron lifetimes are stored in a histogram. It results for the absolute values of the time derivative in the positron annihilation lifetime spectrum N[t]. Each positron lifetime component corresponds to a specific annihilation state in the sample. Not all of these annihilation states are relevant to structural information of the studied material. Thus, the decomposition of the positron annihilation lifetime spectrum into individual components is crucial for isolating the data describing material defects, e.g., polymer free volume. The experimentally recorded time distribution is, due to the errors of the instrumentation, convoluted with the resolution function R[t − t0] and has to be corrected additionally by the uncorrelated background b. It results in:

$$N[t] = BG + N_{tot} \sum_{i=1}^{K_P} \frac{I_i^P}{\tau_i} \exp\left(-\frac{t-t_0}{\tau_i}\right) R[t-t_0] \qquad (2)$$

with

$$R[t-t_0] = \sum_{j=1}^{K_G} \frac{I_j^G}{\sqrt{2\pi}\sigma_j} \exp\left(-\frac{(t-\mu_j)^2}{2\sigma_j^2}\right) \qquad (3)$$

N_{tot} – Histogram overall statistics

BG – Background

t_0 – time shift of the spectrum

$R[t- t_0]$ – Resolution function

K_G – Number of Gaussian functions

I_j^G – Intensities of the Gaussian function

μ_j – Time shift of the Gaussian function

σ_j – Resolution of the system

The time resolution of the spectrometer is described by two Gaussian functions which were determined by a reference measurement.

S.5. Tao Eldrup Model

The general TE model can be used to estimate the sizes of material voids (e.g., polymer free volume elements) based on the experimentally measured positron lifetimes based on the semiempirical equation below:

$$\tau = \frac{1}{2}\left[1 - \frac{R}{R+d} + \frac{1}{2\pi}\sin\left(\frac{2\pi r}{R+d}\right)\right] \qquad (4)$$

τ – positronium lifetime (ns)

R – radius of the free volume elements (nm)

d – electron layer thickness (0.1656 nm)

S.6. Positron Lifetime Components

Table S.4. Positron lifetimes (τ) and lifetime intensities (I) for EW and LW samples.

EW 1-2										
RH (%)	τ_1 (ns)	τ_2 (ns)	τ_3 (ns)	τ_4 (ns)	τ_5 (ns)	I_1 (%)	I_2 (%)	I_3 (%)	I_4 (%)	I_5 (%)
1.3	0.269	0.382	0.460	1.745 (0.01)	2.52	35.11 (0.35)	8.0	40.15 (0.47)	16.24 (0.29)	0.5
12.5	0.269	0.382	0.460	1.682 (0.01)	2.52	35.21 (0.26)	8.0	43.00 (0.33)	13.29 (0.24)	0.5
39.3	0.269	0.382	0.460	1.733 (0.01)	2.52	35.04 (0.28)	8.0	44.93 (0.37)	11.53 (0.12)	0.5
54.9	0.269	0.382	0.460	1.826 (0.01)	2.52	34.55 (0.22)	8.0	45.85 (0.27)	11.10 (0.07)	0.5
80.9	0.269	0.382	0.460	1.877 (0.01)	2.52	34.13 (0.24)	8.0	46.05 (0.29)	11.30 (0.10)	0.5

EW 3-4										
RH (%)	τ_1 (ns)	τ_2 (ns)	τ_3 (ns)	τ_4 (ns)	τ_5 (ns)	I_1 (%)	I_2 (%)	I_3 (%)	I_4 (%)	I_5 (%)
1.9	0.269	0.382	0.460	1.757 (0.01)	2.52	35.10 (0.80)	8.0	40.25 (0.80)	16.14 (0.27)	0.5
12.1	0.269	0.382	0.460	1.691 (0.01)	2.52	35.22 (0.36)	8.0	42.98 (0.36)	13.30 (0.16)	0.5
38	0.269	0.382	0.460	1.739 (0.01)	2.52	34.93 (0.33)	8.0	45.09 (0.33)	11.47 (0.10)	0.5
56.6	0.269	0.382	0.460	1.820 (0.01)	2.52	34.86 (0.38)	8.0	45.61 (0.38)	11.03 (0.11)	0.5
75.2	0.269	0.382	0.460	1.857 (0.01)	2.52	34.34 (0.35)	8.0	45.62 (0.35)	11.54 (0.10)	0.5

LW 1-2										
RH (%)	τ_1 (ns)	τ_2 (ns)	τ_3 (ns)	τ_4 (ns)	τ_5 (ns)	I_1 (%)	I_2 (%)	I_3 (%)	I_4 (%)	I_5 (%)
0.8	0.247	0.382	0.434	1.739 (0.01)	2.52	26.55 (0.16)	8.0	48.52 (0.24)	16.42 (0.11)	0.5

12	0.247	0.382	0.434	1.611 (0.01)	2.52	26.91 (0.26)	8.0	51.77 (0.35)	12.81 (0.13)	0.5
39.8	0.247	0.382	0.434	1.668 (0.01)	2.52	26.70 (0.24)	8.0	53.81 (0.29)	10.99 (0.10)	0.5
67.5	0.247	0.382	0.434	1.742 (0.01)	2.52	26.07 (0.26)	8.0	54.89 (0.32)	10.54 (0.08)	0.5

LW 3-4										
RH (%)	τ_1 (ns)	τ_2 (ns)	τ_3 (ns)	τ_4 (ns)	τ_5 (ns)	I_1 (%)	I_2 (%)	I_3 (%)	I_4 (%)	I_5 (%)
1	0.247	0.382	0.434	1.723 (0.01)	2.52	26.77 (0.23)	8.0	48.13 (0.30)	16.60 (0.10)	0.5
12	0.247	0.382	0.434	1.612 (0.01)	2.52	27.07 (0.27)	8.0	51.72 (0.34)	12.70 (0.11)	0.5
40.4	0.247	0.382	0.434	1.674 (0.01)	2.52	26.48 (0.32)	8.0	54.14 (0.34)	10.88 (0.06)	0.5
70.9	0.247	0.382	0.434	1.767 (0.01)	2.52	26.00 (0.31)	8.0	54.92 (0.38)	10.57 (0.10)	0.5

S.7. PALS Desorption Experiment

In addition to the experiment described in the study, we performed kinetic PALS measurements in desorption, starting from water-saturated sample states. The measurements were performed at 95, 85, and 75% RH.

The figure S.2 displays τ4 kinetic data measured after the sample equilibrium was assumed, i.e., 24 hours after the PALS measurement was started. It can be seen that τ_4 values correspond to o-Ps annihilation in liquid water at room temperature at all measured RHs. In other words, o-Ps annihilation signal likely originates primarily from water clusters present in the cell walls at high cell wall moisture content. The figure S.3 displays corresponding Int_4 values.

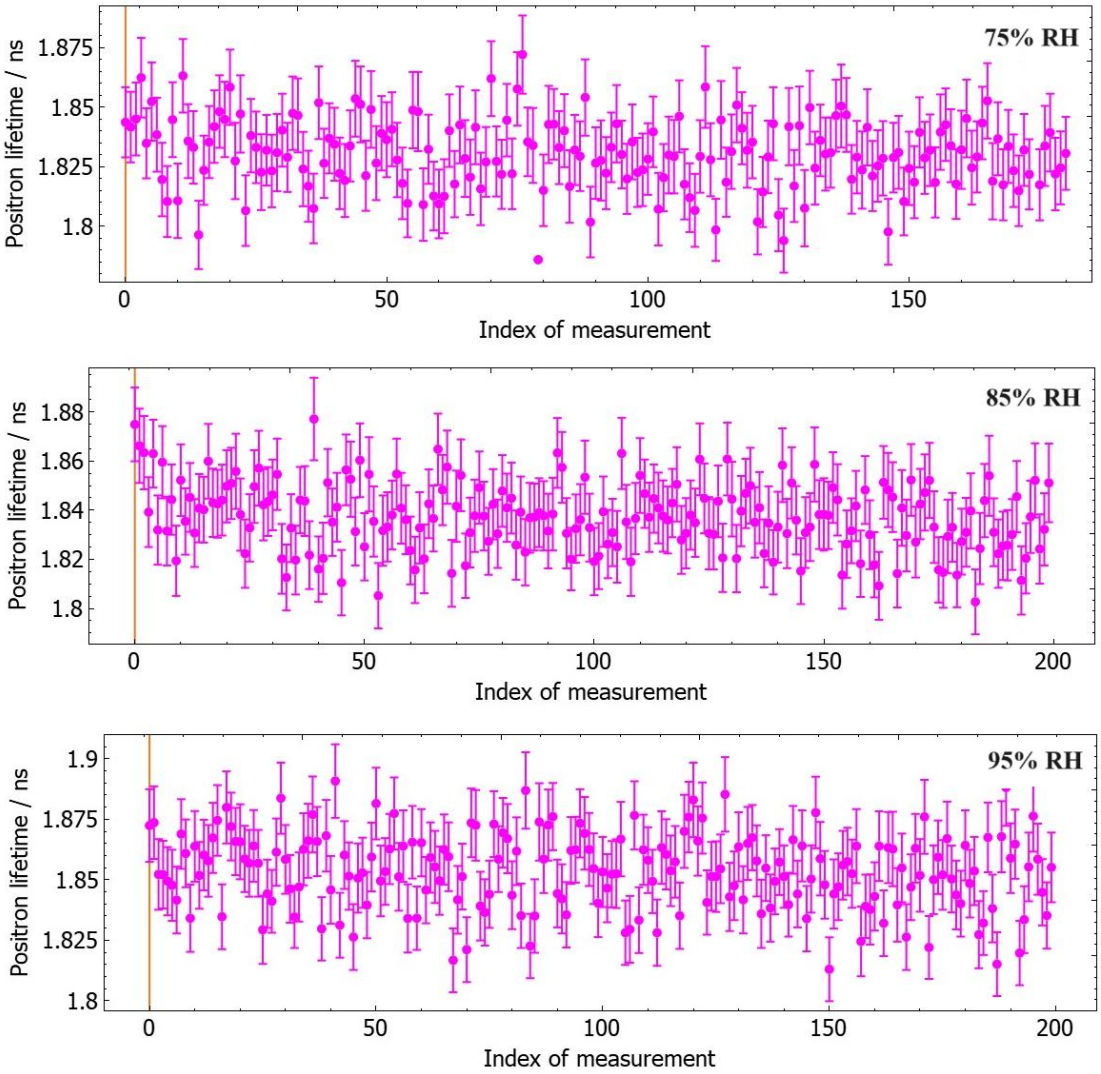

Fig. S.2 *Kinetic measurements of mean τ_4 lifetime at 75, 85 and 95% RH.*

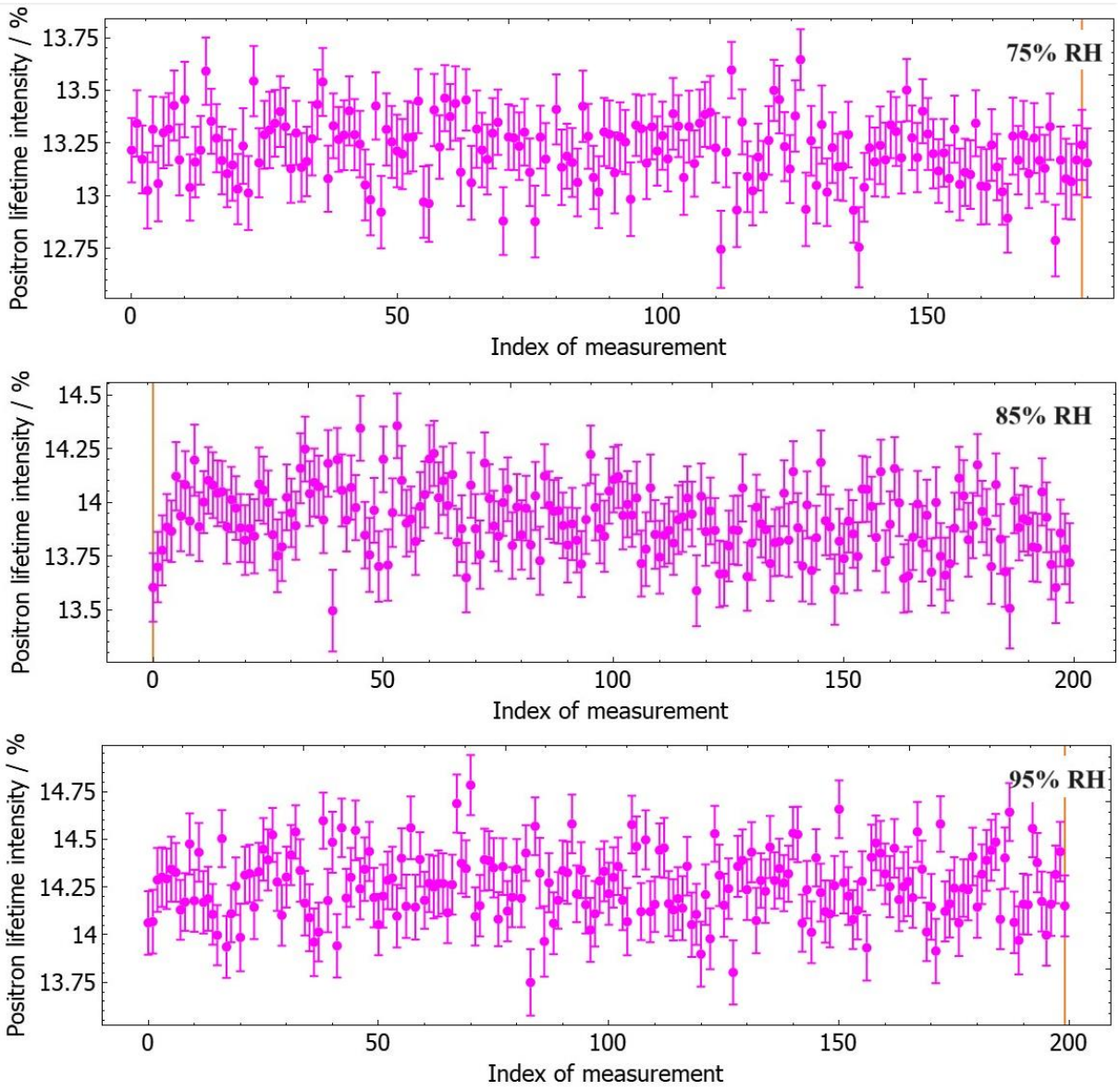

Fig. S.3 *Kinetic measurements of mean I_4 lifetime at 75, 85 and 95% RH.*

Literature

Brandt W, Paulin R (1977) Positron implantation-profile effects in solids. Phys Rev B 15(5):2511–2518. https://doi.org/10.1103/PhysRevB.15.2511

Chong L, Cao X, Fuyan L, Zhang P, Zhang Z, Wei L, Wang B (2019) Effect of tissue density on PET spatial resolution in magnetic environment. European Physical Journal Plus 135. https://doi.org/10.1140/epjp/s13360-020-00198-x

Robles JMC, Ogando E, Plazaola F (2007) Positron lifetime calculation for the elements of the periodic table. J Phys: Condens Matter 19(17):176222. https://doi.org/10.1088/0953-8984/19/17/176222